An effective prediction of biomagnification factors for organochlorine pollutants

Ming Cai Zhang
Lanzhou University
Hong Lin Zhai (zhaihl@163.com)
Lanzhou University https://orcid.org/0000-0001-7088-4962
Ke Xin Bi
Lanzhou University
Bin Qiang Zhao
Lanzhou University
Hai Ping Shao
Lanzhou University

Research Article

Keywords: Biomagnification factors (BMF), Organochlorine pollutants, molecular structure, Tchebichef image moment (TM), Quantitative structure-property relationship (QSPR)

Posted Date: March 3rd, 2021

DOI: https://doi.org/10.21203/rs.3.rs-243149/v2

An effective prediction of biomagnification factors for organochlorine pollutants

Ming Cai Zhang, Hong Lin Zhai*, Ke Xin Bi, Bin Qiang Zhao, Hai Ping Shao

College of Chemistry & Chemical Engineering, Lanzhou University, Lanzhou, 730000, PR China

Abstract

Biomagnification factor (BMF) is an important index of pollutants in food chains but its experimental determination is quite tedious. In this contribution, as the feature descriptors of molecular information, Tchebichef moments (TMs) were calculated from their structural images. Then stepwise regression was employed to establish the prediction model for the *logBMF* of organochlorine pollutants. The correlation coefficient with leave-one-out cross-validation (R_{cv}) was 0.9570; the correlation coefficient of prediction (R_p) and root mean square error ($RMSE_p$) for external independent test set reached 0.9594 and 0.2129, respectively. Compared with traditional two-dimensional (2D) quantitative structure-property relationship (QSPR) and the reported augmented multivariate image analysis applied to QSPR (aug-MIA-QSPR), the proposed approach is more simple, accurate and reliable. This study not only obtained the model with better stability and predictive ability for the BMF of organochlorine pollutants, but also provided another effective approach to QSPR research.

Keywords: Biomagnification factors (BMF); Organochlorine pollutants; molecular structure; Tchebichef image moment (TM); Quantitative structure-property relationship (QSPR)

* Correspondence to: Tel.: +86 931 8912596; fax: +86 931 8912582; E-mail address: zhaihl@163.com (H.L. Zhai).

1. Introduction

With the developments of modern industries, the problem of environmental pollution has been more and more payed attention because that influences human health. Persistent organic pollutions (POPs) are one of the main factors contributing to environmental pollutions, which include three categories: certain industrial chemicals, certain by-products and contaminants, and certain industrial processes (Hillman 1998). A great many POPs are organochlorine compounds (Rosa Vilanova 2001) that easily circulate into organisms with ecosystem cycles (both on land and in aquatic environments), which causes damage to the physiological function of the organisms (Jepson et al. 2016, Paul D. Jepson 2009). More important, since the increasing rate of their concentration is higher than that of degradation due to their stability, organochlorine pollutants can be accumulated along the food chains, which causes a toxicity magnification in the organisms at the top of the food chains (also called Biomagnification phenomenon) (Birgit M. Braune 1989). According to one research of the Lake Ontario ecosystem, it was observed that the content of polychlorinated biphenyls (PCBs) increased with trophic levels (Nliml 1988). To assess this toxicity of POPs, biomagnification factor (BMF) was defined and calculated by the following formula (D. Mackay 2000):

$$BMF = \frac{c_B}{c_A} \tag{1}$$

where c_B is the concentration of chemical in the organism and c_A is the concentration in the organism's diet.

Although the BMFs can be determined by the experimental approaches (Charles J. Henny 2003, Serrano et al. 2008, Woodburn et al. 2013), there are very cumbersome, time consuming and needs

very specific facilities. Fortunately, quantitative structure-property relationship (QSPR) is one of useful strategies and has been widely applied in various fields (Dearden 2016, Gramatica 2020). Several QSPR methods had been used to the prediction of BMF. After calculation a large number of molecular descriptors, the most significant descriptors related to BMF were selected by genetic algorithm and used to build the predictive model of artificial neural network (Fatemi &Baher 2009). To overcome the limited experimental data and avoid more animal testing, the BMF of PBDEs was assessed by means of QSAR (Mansouri et al. 2012). Augmented multivariate Image Analysis applied to QSPR (aug-MIA-QSPR) approach was reported to predict the BMFs of aromatic organochlorine pollutants (da Mota et al. 2017). Acceptable-by-design QSAR method to predict the dietary BMF of organic chemicals in fish, in which two kinds of variable selection methods including genetic algorithms and reshaped sequential replacement were employed (Grisoni et al. 2019). In our opinion, the extraction and selection of features are the most important and key steps in QSAR/QSPR research.

Image moment firstly proposed by Hu (Hu 1962) is one of the description methods for grayscale images. Thereafter, a series of image moments have been developed such as Zernike (Teague 1980), Tchebichef (Ramakrishnan Mukundan 2001) and Krawtchouk (Yap et al. 2003) moments. Although these moments are often used to the de-noising or compression in digital image processing, several image moments have been applied to the feature extraction of target information from chemical spectra and employed to establish the analytical models owing to their powerful multi-resolution as well as good invariance (Zhai et al. 2018). As an excellent member of moment family, Tchebichef image moment (TM, also called Chebyshev moment) possesses the more advantages of feature extraction in the analyses of chemical images.

In this study, as the novel descriptors of chemical structures, TMs were calculated directly from the gray images of molecular structures of organochlorine compounds, and stepwise regression was employed to establish the linear model for the prediction of BMF. The performance of the obtained model was evaluated comprehensively. Furthermore, the results from our approach were compared with that of other methods.

2. Data and methods

2.1 Data set

The data set was derived from the literatures (da Mota et al. 2017), which consisted of 30 polychlorinated biphenyls (PCBs) congeners and 10 organochlorine pesticides (DDT, DDE, HCB, TCDF, OCDF, TCDD, H6CDD, H7CDD, OCDD and DDD). It was based on the research of *BMFs* of osprey eggs and whole fish from Willamette River in western Oregon of USA. Their values of *logBMF* are listed in Table 1 as Exp. column. All of 40 samples were randomly divided into training set (30 samples) and test set (10 samples). The training set was used to establish the prediction model, and the test set was employed to evaluate the prediction capability of the obtained model as external independent sample set.

(Table 1)

2.2 Methods

2.2.1 Images of molecular structures

The two-dimensional (2D) molecular structures of the 40 compounds were drawn in ChemBioDraw (v12) software with default conditions (Fixed Length: 1.058 cm, Line Width: 0.035 cm, Bond Spacing: 12% of length, Hash Spacing: 0.095 cm, Font: Times New Roman, Size: 12)

and saved as the grayscale BMP format with the size of 303 pixels × 258 pixels under the resolution ratio of 96 DPI.

2.2.2 Calculation of Tchebichef image moments

For a given grayscale image with size of $N \times M$, the TM can be calculated using the following formula (Bayraktar et al. 2007):

$$T_{n,m} = \frac{1}{\tilde{\rho}(n,N)\tilde{\rho}(m,M)} \sum_{x=0}^{N-1} \sum_{y=0}^{M-1} \tilde{t}_n(x) \tilde{t}_m(y) f(x,y) \quad (n = 0,1,2,\ldots N-1, \quad m = 0,1,2,\ldots M-1) \tag{2}$$

where $\tilde{t}_n(x)$ and $\tilde{t}_m(y)$ are the normalized discrete Tchebichef polynomial of degree n and m, respectively; $\tilde{\rho}(n,N)$ is the squared-norm of the normalized polynomials and $f(x,y)$ is the image intensity function.

Thus the reconstruction of image by $T_{n,m}$ can be performed:

$$\hat{f}(x,y) = \sum_{n=0}^{nN} \sum_{m=0}^{mM} T_{nm} \tilde{t}_n(x) \tilde{t}_m(y) \tag{3}$$

where $\hat{f}(x,y)$ is the reconstructed image, nN and mM are the maximum orders of n and m (n=0-nN, nN<N-1; m=0-mM, mM<M-1). The reconstruction error ε can be calculated:

$$\varepsilon = \sum_{x=0}^{N-1} \sum_{y=0}^{M-1} \left| f(x,y) - \hat{f}(x,y) \right| \tag{4}$$

2.2.3 Modeling and evaluation

Stepwise regression was employed to establish the linear prediction model, in which TMs were regarded as the independent variables and *logBMF* was denoted as dependent variable. The performance of obtained model was evaluated by means of various statistical parameters such as the determination coefficient (R_c), the adjusted determination coefficient (R_{adj}), root mean square error ($RMSE_c$), the correlation coefficient with leave-one-out (LOO) cross-validation (R_{cv}) and LOO

root mean square error ($RMSE_{cv}$) for training set; *F*-test for model and *t*-test for the regression coefficients; the correlation coefficient of test set (R_p) and root mean square error ($RMSE_p$) for test set (Gadaleta et al. 2016).

In order to further inspect the robustness of the model, a randomized test was performed on the established model, in which models are established with invariant *X*-matrix and randomized *Y*-matrix (Mitra et al. 2010). To determine the reliable of model, ${}^cR_P^2$ was adopted by following corrected formula (Todeschini 2010):

$$ {}^cR_p^2 = R\sqrt{\left(R^2 - R_r^2\right)} \tag{5}$$

where R is R_c of the model and R_r^2 is the average of R^2 for the randomized model.

The predictive capability of the model can be validated by external test, and the related parameters (k, k', r_m^2, $r_m'^2$ and Δr_m^2) are defined by follows (Ojha et al. 2011, Roy et al. 2013):

$$k = \frac{\sum\left(Y_{obs} \times Y_{pred}\right)}{\sum\left(Y_{pred}\right)^2} \tag{6}$$

$$k' = \frac{\sum\left(Y_{obs} \times Y_{pred}\right)}{\sum\left(Y_{obs}\right)^2} \tag{7}$$

$$r_m^2 = r^2\left(1 - \sqrt{r^2 - r_0^2}\right) \tag{8}$$

$$r_m'^2 = r^2\left(1 - \sqrt{r^2 - r_0'^2}\right) \tag{9}$$

$$\Delta r_m^2 = \left|r_m^2 - r_m'^2\right| \tag{10}$$

Here, k and k' is the slope of experimental and predicted values respectively. Y_{obs} and Y_{pred} are the observed and predicted values, respectively. r_m^2 and $r_m'^2$ are modified r^2. r^2 and $r_0'^2$ are determination coefficients between the observed and predicted values for the least square linear regression with and without interpret. And Δr_m^2 is the absolute of the difference between them.

Meanwhile, it is necessary to discuss the applicability domain (AD) of the established model

126 to study its scope and limitations. In this work, Williams plot was employed to calculate the
127 applicability domain (AD) of the established model, which presents the relationship between
128 leverage (Hat matrix) and standardized residuals, and Hat matrix could be calculated by the
129 following relation (P. 2007):

130 $$H = X(X^T X)^{-1} X^T \quad (11)$$

131 where X is the matrix composed of descriptors in the established model and T means the transpose
132 matrix. In general, the threshold H^* of H is equal to $3p/n$ (n is the number of training set sample and
133 p is the established model's variables number plus one), and the standardized residuals are normally
134 accepted within the range ±3 (Roy et al. 2015).

135 2.2.4 Comparison with 2D QSPR as well as the reported method

136 Traditional 2D QSPR method was also applied to the same data set. The molecular descriptors
137 of the 40 samples were calculated by CODESSA (v2.63) after being optimized by HyperChem
138 (v7.5), and the total of 337 common descriptors were obtained (Supporting information, Table S1).
139 A linear QSPR model was established by stepwise regression based on the training set, and used to
140 the prediction of the test set. The obtained results were compared with that of the proposed method.

141 The proposed TM model was also applied to predict the *logBMF* of the samples in the five
142 different test sets as same as the reference (da Mota et al. 2017), and the calculated results were
143 compared with that of the method in this reference.

144

145 **3. Results and discussions**

146 3.1 Characteristic of Tchebichef image moments

147 Owing to the excellent description ability with multi-resolution and invariance properties in

148 image processing, Tchebichef image moment (TM) is an important image characteristic based on
149 the discrete orthogonal polynomials (Ramakrishnan Mukundan 2001). What is more, no numerical
150 approximation is needed during the calculation.

151 TMs with different moment orders represent different information in image according to Eq. 2,
152 which can decompose the information of molecular structure image (multi-resolution ability). Then
153 the important features ($T_{n,m}$) related to the BMF of chemical compounds could be selected by
154 stepwise regression to establish the prediction model. Owing to its invariance property in the image
155 operation of shifting, scaling and rotation, TMs have relative stability of the calculated values, which
156 means that molecular structures do not need to be precisely aligned in their images.

157 3.2 Model and evaluation

158 After the TMs were directly calculated from the grayscale images of molecular structures, the
159 maximum orders were determined as nN=28 and mM=43 according to the change of reconstruction
160 errors (Eq. 4). Then a linear quantitative model was established by stepwise regression based on the
161 training set, in which the TMs were the independent variables and *logBMF* was the target response
162 variable. The values of TMs in the following model are listed in Table S2.

163
$$log\ BMF = -1.0732 + 92.1940 \times T_{1,1} - 6.9062 \times T_{4,14} - 10.2245 \times T_{13,9} - 5.5451 \times T_{13,12} + 14.7530 \times T_{13,27}$$

164 The calculated *logBMF* values of all samples are listed Table 1 and the statistical parameters
165 of the established model are summarized in Table 2. The linear relationship between the calculated
166 values and the experimental values are shown in Fig. 1. From Table 2, the R_c (0.9726), R_{adj} (0.9668)
167 and $RMSE_c$ (0.1052) were satisfactory, which indicates that the model was accurate; R_{cv} (0.9570)
168 and $RMSE_{cv}$ (0.1320) suggested that there was not over-fitting; the p-value of F-test (2.08e-14)

showed the good linear relationship between the independent variables and response variable in this model, and the results of *t*-test ensured that the regression coefficients had statistical significance. For the test set, R_p (0.9594) and $RMSE_p$ (0.2129) represented that the established model possessed satisfactory predictive ability. All above statistical parameters indicated that the model had high reliability and accuracy.

(Table 2, Fig. 1)

To investigate the robustness and reliability of the TM model, the further evaluation was carried out. For randomized test, the parameter ${}^{c}R_P^2$ is 0.5988 (more than its threshold value of 0.5), indicating that the model has not randomness and fortuitousness. For the external test, the obtained parameters (listed in Table 2) also conform to the requirements ($0.85 \le k \le 1.15$; $0.85 \le k' \le 1.15$; $r_m^2 \ge 0.5$; $r_m'^2 \ge 0.5$; $\Delta r_m^2 \le 0.2$) (Ojha et al. 2011). Besides, Williams plot is shown Fig. 2A. As it could be observed, sample **8** (1, 2, 3, 4, 6, 7, 8, 9-Octachlorodibenzofuran) of the training set and sample **1** (2378TCDF) of test set are outliers with high leverage. Compared with the structures of other chemicals in dataset, sample **8** may be different with others so that they are not well modeled by adopted variables. Another possible reason is the sample belongs to other type chemicals. To the sample **1**, it owns the same structure with sample **8** so that the model may not well predict the value of *logBMF* of it.

(Fig. 2)

All above results and discussions indicated that the proposed method was reliable and reasonable, and the established model possessed the higher robustness and prediction ability.

3.3 Comparison with other methods

3.3.1 Comparison with 2D-QSPR method

191 Based on the 337 common molecular descriptors, the prediction model was established by

192 stepwise regression as follows:

193 $$\begin{aligned} log\ BMF = {} & 57.2032 + 0.0105 \times X_{39} - 0.3412 \times X_{162} - 499.8468 \times X_{174} + 20.8516 \times X_{176} \\ & -42.3347 \times X_{276} - 36.4478 \times X_{327} \end{aligned}$$

194 where X_{39}, Wiener index; X_{162}, No. of occupied electronic levels; X_{174}, Avgnucleoph. react. Index

195 for a Cl atom; X_{176}, Max eletroph. react. index for a C atom; X_{276}, Avg bond order of a Cl atom; X_{327},

196 Principal moment of inertia A.

197 The calculated values of *logBMF* are also listed in Table 1. The obtained statistical parameters

198 (listed in Table 2) and Williams plot (showed in Fig.2B) illustrate that the established 2D-QSPR

199 model was robust and reliable. The comparison of statistical parameters in the Table 2 indicated that

200 the TM model was slightly better than the 2D-QSPR model the owing to its higher prediction ability,

201 which suggested the feasibility of the proposed approach.

202 3.3.2 Comparison with the method in reference

203 Compared with the best results obtained by aug-MIA-QSPR$_{color}$ method in the literature (da

204 Mota et al. 2017), the statistical parameters (listed in Table 2) of the TM model had the more satisfied.

205 For the five different test sets (named test **1**~**5**) used in this literature, the established TM model was

206 also applied to predict the *logBMF* values of the samples, respectively. The obtained statistical

207 parameters R_p^2 and $RMSE_p$ are shown in Table 3. It can be seen that the predicted results from the

208 proposed model are significantly better than that of aug-MIA-QSPR$_{color}$ model, which demonstrates

209 that the proposed model possesses stronger predictive ability and reliability.

210 **(Table 3)**

211

4. Conclusion

In this study, TM method was used to extract the feature information of molecular structure images and establish the linear quantitative model to predict the log*BMF* of organochlorine pollutants. The results of comprehensive evaluation indicate that the established model has satisfactory robustness and predictive ability. As an effective extraction pathway of feature information, TM method could be applied on many QSPR research.

Acknowledgement

This research did not receive any specific grant from funding agencies.

Availability of data and materials

The datasets used and analyzed during the current study are available from the corresponding author on reasonable request.

Compliance with ethical standards

Ethics approval and consent to participate Not applicable.

Consent to publish Not applicable.

Authors Contributions *Ming Cai Zhang***:** Conceptualization, Methodology, Software, Writing- Original draft preparation; *Hong Lin Zhai:* Supervision, Writing- Reviewing and Editing; *Ke Xin Bi* and *Bin Qiang Zhao*: Methodology, Software, Validation; *Hai Ping Shao*: Software.

Competing interests The authors declare that they have no competing interests.

232 **References**

233 Bayraktar B, Bernas T, Robinson JP, Rajwa B (2007): A numerical recipe for accurate image
234 reconstruction from discrete orthogonal moments. Pattern Recognition 40, 659-669

235 Birgit M. Braune RJN (1989): Dynamics of organochlorine compounds in herring gulls: III. Tissue
236 distribution and bioaccumulation in lake ontario gulls. Environmental Toxicology and
237 Chemistry 8, 957-968

238 Charles J. Henny JLK, Robert A. Grove, V. Raymond Bentley and John E. Elliott (2003):
239 Biomagnification Factors (Fish to Osprey Eggs from Willamette River, Oregon, U.S.A.) for
240 PCDDs, PCDFs, PCBs and OC Pesticides Environmental Monitoring & Assessment 84, 275-
241 315

242 D. Mackay AF (2000): Bioaccumulation of persistent organic chemicals: mechanisms and models.
243 Environmental Pollution 110, 375-391

244 da Mota EG, Duarte MH, Barigye SJ, Ramalho TC, Freitas MP (2017): Exploring MIA-QSPR's for
245 the modeling of biomagnification factors of aromatic organochlorine pollutants. Ecotoxicology
246 and environmental safety 135, 130-136

247 Dearden JC (2016): The History and Development of Quantitative Structure-Activity Relationships
248 (QSARs). International Journal of Quantitative Structure-Property Relationships 1, 1-44

249 Fatemi MH, Baher E (2009): A novel quantitative structure-activity relationship model for
250 prediction of biomagnification factor of some organochlorine pollutants. Molecular diversity
251 13, 343-352

252 Gadaleta D, Mangiatordi GF, Catto M, Carotti A, Nicolotti O (2016): Applicability Domain for
253 QSAR Models. International Journal of Quantitative Structure-Property Relationships 1, 45-
254 63

255 Gramatica P (2020): Principles of QSAR Modeling: Comments and Suggestions From Personal
256 Experience. International Journal of Quantitative Structure-Property Relationships 5, 61-97

257 Grisoni F, Consonni V, Vighi M (2019): Acceptable-by-design QSARs to predict the dietary
258 biomagnification of organic chemicals in fish. Integrated Environmental Assessment and
259 Management 15, 51-63

Hillman K (1998): United Nations Economic Commission for Europe: Draft Protocol to the Convention on Long-range Transboundary Air Pollution on Persistent Organic Pollutants*. International Legal Materials 37, 505-529

Hu M-K (1962): Visual pattern recognition by moment invariants IRE Transactions on Information Theory 8, 179-187

Jepson PD et al. (2016): PCB pollution continues to impact populations of orcas and other dolphins in European waters. Sci Rep 6, 18573

Mansouri K, Consonni V, Durjava MK, Kolar B, Oberg T, Todeschini R (2012): Assessing bioaccumulation of polybrominated diphenyl ethers for aquatic species by QSAR modeling. Chemosphere 89, 433-44

Mitra I, Saha A, Roy K (2010): Exploring quantitative structure–activity relationship studies of antioxidant phenolic compounds obtained from traditional Chinese medicinal plants. Molecular Simulation 36, 1067-1079

Nliml BGOaAJ (1988): Trophodynamic analysis of polychlorinated biphenyl congeners and other chlorinated hydrocarbons in the Lake Ontario ecosystem. Environ Sci Technol 22, 388-397

Ojha PK, Mitra I, Das RN, Roy K (2011): Further exploring rm2 metrics for validation of QSPR models. Chemometrics and Intelligent Laboratory Systems 107, 194-205

P. G (2007): Principles of QSAR models validation: Internal and external. QSAR & Combinatorial Science 26, 694-701

Paul D. Jepson PMB, Robert Deaville, Colin R. Allchin, John R. Baker, Robin J. Law (2009): Relationships between polychlorinated biphenyls and health status in harbor porpoises (Phocoena phocoena) stranded in the United Kingdom Environmental Toxicology and Chemistry 24, 238-248

Ramakrishnan Mukundan S-HO, P.A. Lee (2001): Image analysis by Tchebichef moments. IEEE Transactions on Image Processing 10, 1357-64

Rosa Vilanova PFn, Carolina Martı´nez, and Joan O. Grimalt (2001): Organochlorine Pollutants in Remote Mountain Lake Waters. Journal of Environmental Quality 30, 1286-1295

Roy K, Chakraborty P, Mitra I, Ojha PK, Kar S, Das RN (2013): Some case studies on application of "r(m)2" metrics for judging quality of quantitative structure-activity relationship predictions:

289 emphasis on scaling of response data. J Comput Chem 34, 1071-82
290 Roy K, Kar S, Ambure P (2015): On a simple approach for determining applicability domain of
291 QSAR models. Chemometrics and Intelligent Laboratory Systems 145, 22-29
292 Serrano R, Blanes MA, Lopez FJ (2008): Biomagnification of organochlorine pollutants in farmed
293 and wild gilthead sea bream (Sparus aurata) and stable isotope characterization of the trophic
294 chains. Sci Total Environ 389, 340-9
295 Teague MR (1980): Image analysis via the general theory of moments Journal of the Optical Society
296 of America 70, 920-930
297 Todeschini R (2010): Milano Chemometrics. University of MilanoBicocca, Milano, Italy (personal
298 communication)
299 Woodburn K, Drottar K, Domoradzki J, Durham J, McNett D, Jezowski R (2013): Determination
300 of the dietary biomagnification of octamethylcyclotetrasiloxane and
301 decamethylcyclopentasiloxane with the rainbow trout (Oncorhynchus mykiss). Chemosphere
302 93, 779-88
303 Yap PT, Paramesran R, Ong SH (2003): Image analysis by Krawtchouk moments. IEEE Trans Image
304 Process 12, 1367-77
305 Zhai HL, Li BQ, Chen J, Wang X, Xu ML, Liu JJ, Lu SH (2018): Chemical image moments and
306 their applications. TrAC Trends in Analytical Chemistry 103, 119-125
307
308
309

Table Caption:

Table 1 Experimental and predicted *logBMF* values of all samples

Table 2 Performance of the established models

Table 3 Comparison of the predicted results for the five test sets

Figure Caption:

Figure 1 Linear relationship between *logBMF* calculated values and experimental values

Figure 2 Williams plots. (A) TM model (H^*=0.6) (B) 2D-QSPR model (H^*=0.7)

319 **Table 1** Experimental and predicted *logBMF* values of all samples

No.	Compounds	Abbr.	*logBMF*		
			Exp.	*TM*	*2D-QSPR*
1*	2378TCDF	TCDF	-0.12	-0.10	0.31
2	hexachlorobenzene	HCB	0.32	0.31	0.34
3	3,3',4,4'-Tetrachlorobiphenyl	PCB77	0.77	0.82	0.62
4	2,4,4',5-Tetrachlorobiphenyl	PCB74	0.83	0.89	0.96
5*	2,3,4,4'-Tetrachlorobiphenyl	PCB60	0.90	0.95	0.95
6	2,2',3,4',5',6-Hexachlorobiphenyl	PCB149	0.95	0.97	1.02
7	2,2',3,3',4,5,6'-Heptachlorobiphenyl	PCB174	1.00	1.11	1.12
8	1,2,3,4,6,7,8,9-Octachlorodibenzofuran	OCDF	1.00	0.97	1.06
9*	2,3,3',4',6-Pentachlorobiphenyl	PCB110	1.04	0.96	1.31
10	2,2',4,4',5-Pentachlorobiphenyl	PCB99	1.11	1.15	1.24
11	2,2',4,5,5'-Pentachlorobiphenyl	PCB101	1.25	1.18	1.12
12	2,3,7,8-tetrachlorodibenzo-p-dioxin	TCDD	1.25	1.21	1.32
13	2,3',4,4',5-Pentachlorobiphenyl	PCB118	1.30	1.09	1.25
14	3,3',4,4',5,5'-Hexachlorobiphenyl	PCB169	1.32	1.41	1.48
15*	2,3,3',4,4'-Pentachlorobiphenyl	PCB105	1.36	1.14	1.20
16*	2,2',3,3',4,4',6-Heptachlorobiphenyl	PCB171	1.36	0.85	1.44
17	2,2',3,4,5,5'-Hexachlorobiphenyl	PCB141	1.43	1.30	1.39
18	2,2',3,4,4',5',6-Heptachlorobiphenyl	PCB183	1.43	1.52	1.30
19	2,2',3,3',4,4',5,5'-Octachlorobiphenyl	PCB194	1.43	1.55	1.62
20*	2,2',3,4,4',5,5',6-Octachlorobiphenyl	PCB203	1.43	1.46	1.47
21	3,3',4,4',5-Pentachlorobiphenyl	PCB126	1.43	1.31	1.23
22	2,2',3,4,4',5'-Hexachlorobiphenyl	PCB138	1.46	1.34	1.41
23*	2,2',4,4',5,5'-Hexachlorobiphenyl	PCB153	1.46	1.28	1.25
24	2,2',3,4',5,5'-Hexachlorobiphenyl	PCB146	1.48	1.53	1.41
25	2,2',3,3',4,5',6,6'-Octachlorobiphenyl	PCB201	1.48	1.44	1.45
26	2,2',3,3',4,5,6,6'-Octachlorobiphenyl	PCB200	1.50	1.49	1.41
27	2,2',3,3',4,5,5'-Heptachlorobiphenyl	PCB172	1.53	1.40	1.57
28*	2,2',3,4,4',5,5'-Heptachlorobiphenyl	PCB180	1.53	1.45	1.48
29	1,1-Dichloro-2,2-(4-ClC6H4)ethane	p,p'DDD	1.61	1.81	1.67
30*	Dichlorodiphenyltrichloroethane	DDT	1.92	2.02	2.37
31	1,1-Dichloro-2,2-(4-ClC6H4)ethene	p,p'-DDE	2.19	1.96	2.14
32*	1,2,3,6,7,8-Hexachlorodibenzo-p-Dioxin	H6CDD	2.44	2.15	2.11
33	1,2,3,4,6,7,8-Heptachlorodibenzo-p-Dioxin	H7CDD	2.44	2.42	2.33
34	1,2,3,4,6,7,8,9-Octachlorodibenzo-p-Dioxin	OCDD	2.49	2.58	2.48
35	2,3',4,4'-Tetrachlorobiphenyl	PCB66	0.83	1.04	0.93
36	2,2',3,5',6-Pentachlorobiphenyl	PCB95	0.83	0.88	0.83
37	2,2',3,3',4,4',5-Heptachlorobiphenyl	PCB170	1.53	1.46	1.59
38	2,3,3',4,4',5,6-Heptachlorobiphenyl	PCB190	1.53	1.50	1.68

39	2,2',3,4,4',5,6'-Heptachlorobiphenyl	PCB182	1.39	1.47	1.28
40	2,2',3,4',5,5',6-Heptachlorobiphenyl	PCB187	1.39	1.39	1.25

320 Note: The samples with asterisk (*) belong to test set while others belong to training set.

321

Table 2 Performance of the established models

Data set	Item	TM	2D-QSPR
Training set	LV_c	5	6
	R_c	0.9726	0.9732
	R_{adj}	0.9668	0.9661
	R_{cv}	0.9570	0.9545
	$RMSE_c$	0.1052	0.1040
	$RMSE_{cv}$	0.1320	0.1353
	F-test (*p*-value)	2.08E-14	1.56E-13
	R_r^2	0.5669	0.3065
	${}^cR_p^2$	0.5988	0.7790
	MAE_c	0.08	0.09
Test set	R_p	0.9594	0.9236
	$RMSE_p$	0.2129	0.2541
	k	1.0783	0.9757
	k'	0.9129	0.9952
	r_m^2	0.8567	0.7685
	$r_m'^2$	0.9161	0.6220
	Δr_m^2	0.0594	0.1465
	MAE_p	0.16	0.21

Table 3 Comparison of the predicted results for the different test sets

Test set	R_p^2		$RMSE_p$	
	TM	aug-MIA-QSPR$_{color}$	TM	aug-MIA-QSPR$_{color}$
test **1**	0.9710	0.8451	0.0792	0.2310
test **2**	0.9877	0.7808	0.0589	0.2261
test **3**	0.9844	0.8719	0.0803	0.2048
test **4**	0.9854	0.8759	0.0590	0.1957
test **5**	0.9860	0.8978	0.0690	0.2061
Average±SD	0.9829±0.0068	0.8543±0.0452	0.0693±0.0104	0.2127±0.0151

Figure 1

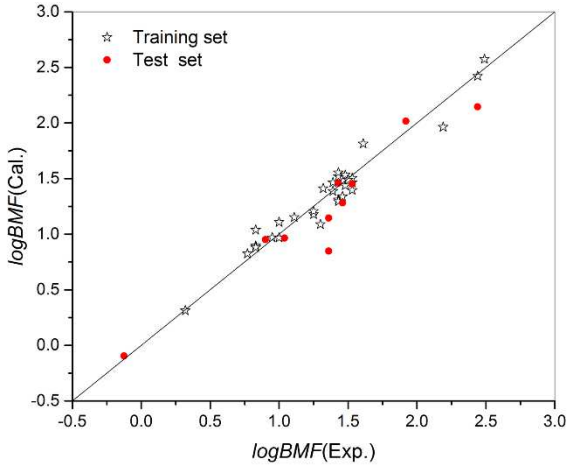

Figure 2

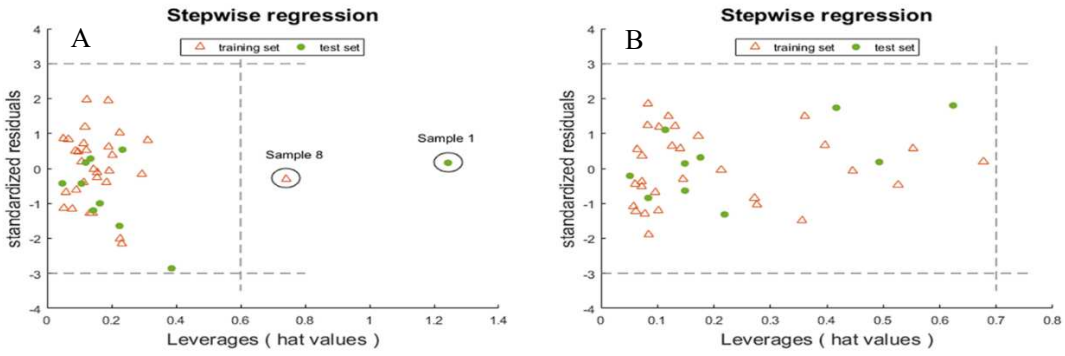

Figures

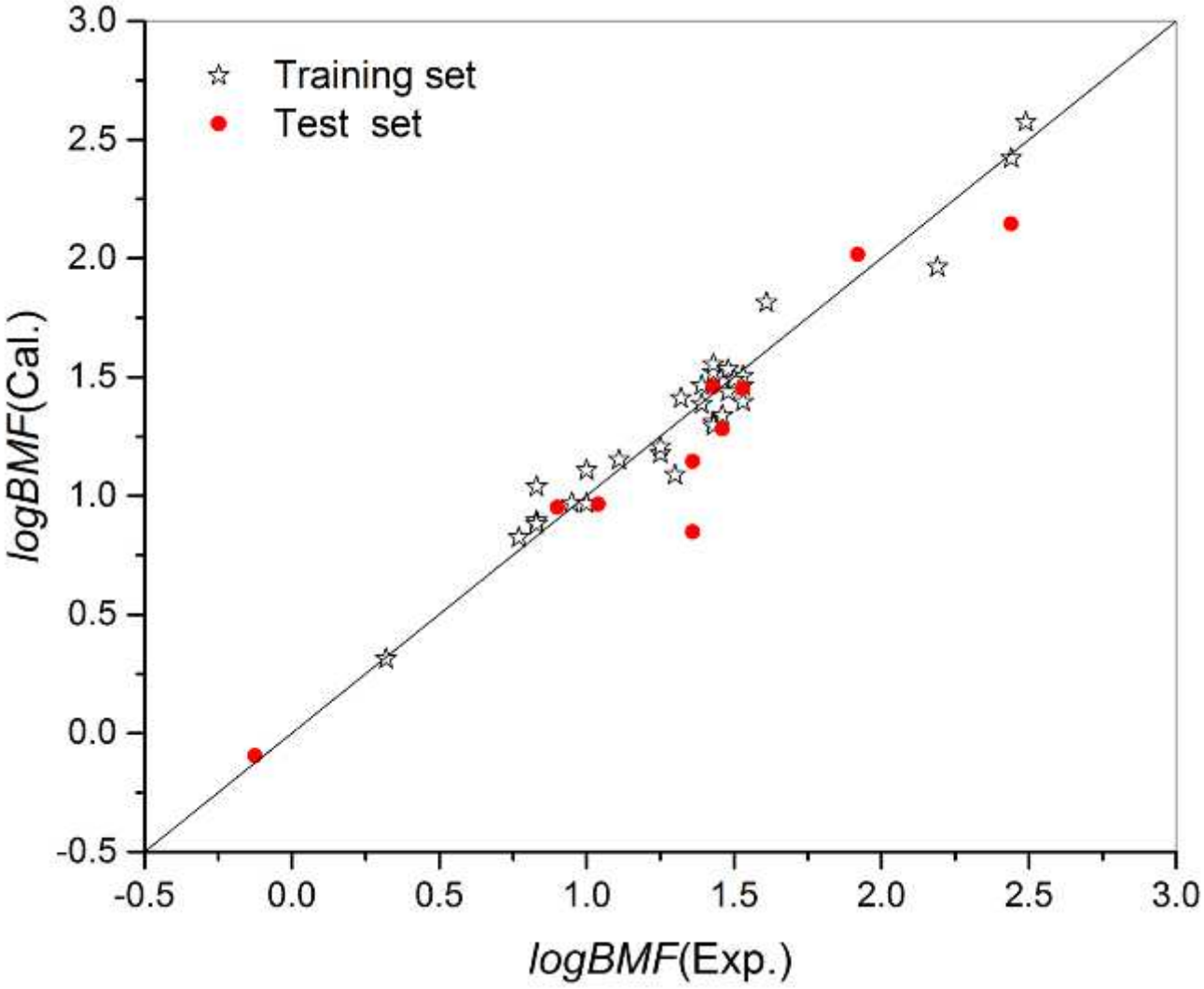

Figure 1

Linear relationship between logBMF calculated values and experimental values

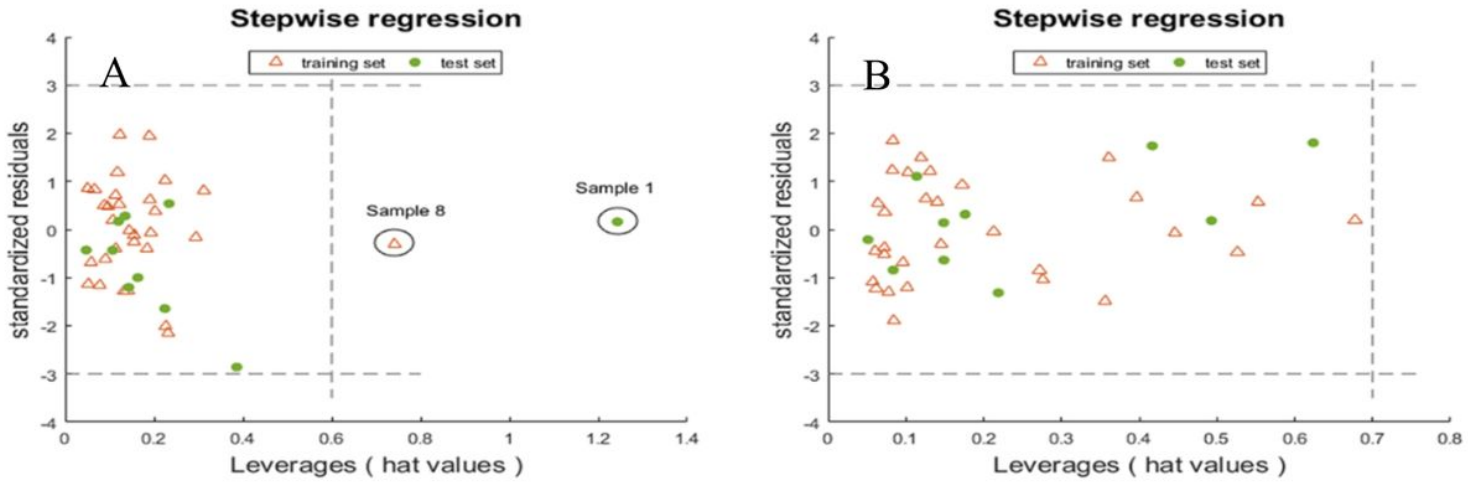

Figure 2

Williams plots. (A) TM model (H*=0.6) (B) 2D-QSPR model (H*=0.7)

Supplementary Files

This is a list of supplementary files associated with this preprint. Click to download.

- SupplementaryInformation.docx